Proceedings of the 7th International Symposium on Cavitation
CAV2009
August 17-22, 2009, Ann Arbor, Michigan, USA

CAV2009-177

DAMAGE POTENTIAL OF THE SHOCK-INDUCED COLLAPSE OF A GAS BUBBLE

Eric Johnsen*
Center for Turbulence Research
Stanford University
Stanford, CA 94305
Email: johnsen@stanford.edu

Tim Colonius
Division of Engineering and
Applied Science
California Institute of Technology
Pasadena, CA 91125
Email: colonius@caltech.edu

Robin Cleveland
Department of Mechanical Engineering
Boston University
Boston, MA 02215
Email: robinc@bu.edu

ABSTRACT

Numerical simulations are used to evaluate the damage potential of the shock-induced collapse of a pre-existing gas bubble near a rigid surface. In the context of shock wave lithotripsy, a medical procedure where focused shock waves are used to pulverize kidney stones, shock-induced bubble collapse represents a potential mechanism by which the shock energy directed at the stone may be amplified and concentrated. First the bubble dynamics of shock-induced collapse are discussed. As an indication of the damage potential, the wall pressure is considered. It is found that, for bubbles initially close to the wall, local pressures greater than 1 GPa are achieved. For larger stand-off distances, the wall pressure is inversely proportional to the location of bubble collapse. From this relationship, it is found that bubbles within a certain initial stand-off distance from the wall amplify the pressure of the incoming shock. Furthermore, the extent along the wall over which the pressure due to bubble collapse is higher than that of the pulse is estimated. In addition, the present computational fluid dynamics simulations are used as input into an elastic waves propagation code, in order to investigate the stresses generated within kidney stone in the context of shock wave lithotripsy. The present work shows that the shock-induced collapse of a gas bubble has potential not only for erosion along the stone surface, but also for structural damage within the stone due to internal wave reflection and interference.

*Address all correspondence to this author.

INTRODUCTION

Shock wave lithotripsy (SWL) is a non-invasive medical procedure in which shock waves are focused on kidney stones in an attempt to break them [2]. A lithotripter pulse consists of a sharp compressive front, followed by a long expansion tail that has a tensile component, as shown in Figure 1. Since kidney stones typically reside in urine and pooled blood, cavitation bubbles form after the passage of the tensile part of the pulse. The exact mechanism responsible for stone comminution has not yet been fully determined; however, two main mechanisms are thought to play an important role: wave propagation within the stone [3, 20] and cavitation erosion along the stone surface [5, 6].

Wave propagation within the stone leads to several kinds of failure. First, shear waves and surface waves resulting from the different speed of propagation of the shock in the fluid and in the stone interfere constructively to form regions of high stresses [3]. Second, it has been postulated that dynamic squeezing due to the pressure wave in the liquid acts as a compressive hoop stress [7]. Finally, lithotripter pulses propagating through the stone invert their amplitude upon reflection off the distal side of the stone [8, 19]; for stones greater than a certain size, this large negative pressure superposes with the tensile part of the incoming pulse, thus creating a magnified tensile region and breaking the stone near the posterior end. Because of the wave reflection within the stone, both of these phenomena are strongly affected by the geometry and size of the stone.

Another process of importance in stone comminution is cavitation erosion. After the passage of the tensile part of the pulse, vapor bubbles grow and gather as a cloud near the stone

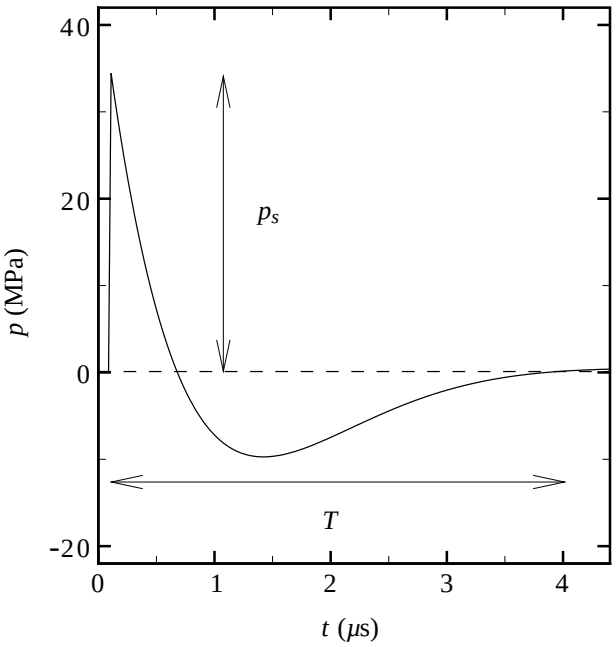

Figure 1. Model lithotripter pulse.

where they collapse as a whole, thereby generating high pressures [15, 19]. Cavitation bubbles collapse because of the pressure difference between the liquid (approximately atmospheric pressure) and the bubble (approximately vapor pressure). When a bubble collapses near a rigid surface, a re-entrant jet directed toward the surface forms on the bubble side farthest from the surface and penetrates the bubble [16]. The direct impact of this jet onto the surface can cause significant damage [14, 17] and has been regarded as the primary cause of cavitation erosion in SWL [5, 6]; for vapor bubble collapse, wall pressures up to 20 MPa have been measured experimentally by Tomita & Shima [17], though Philipp & Lauterborn [14] estimate that wall pressures may be on the order of 1GPa. Another type of bubble collapse is the shock-induced collapse of pre-existing bubbles. Recently, numerical simulations of shock-induced collapse of a gas bubble have shown that pressures on the order of 1 GPa are generated along the stone surface [12, 13, 18], which is much larger than the maximum compressive strength of kidney stones (on the order of 10 MPa [4]). Thus, shock-induced collapse show potential for the erosion of the stone surface. The reason that shock-induced collapse leads to higher pressures than Rayleigh collapse is that the pressure driving the bubble collapse is much larger in the former (approximately 350:1 compared to 35:1 in SWL).

The individual effect of wave propagation within the stone and of cavitation erosion is difficult to assess. However, experiments where either mechanism is suppressed show that the most effective comminution rate is achieved when both mechanisms work in synergy [20]: spallation due to the high tension created by the reflected pulse breaks the stones into smaller fragments, which are further eroded by the bubble collapse. Until this point, the process thought to be responsible for the wave propagation within the stone is the lithotripter pulse; the present work shows that shocks are generated by bubble collapse and that the propagation of these waves may be a source of additional damage within the stone.

The present study discusses two mechanisms by which the lithotripter pulse and bubble collapse work in synergy to achieve the most efficient comminution rate: erosion of the stone surface by bubble collapse and generation of large tensile stresses within the stone. The potential for surface erosion caused by shock-induced collapse is evident, given the high pressures generated along the stone surface [13]. In addition, three important observations made from prior studies of shock-induced collapse [12, 13] form the basis of the present analysis of structural damage within the stone: (i) A radially propagating shock wave is generated upon the non-spherical bubble collapse, (ii) For bubbles close enough to the stone surface, the pressure may be far greater than that of the pulse, and (iii) The amplitude of the emitted shock wave decays as $1/r$. As the shock emitted upon bubble collapse interacts with the stone, part of the shock is transmitted into the stone and part is reflected. Thus effects similar to those due to the propagation of the lithotripter pulse through the stone can be anticipated. Because of the decay in pressure with distance, such an effect is expected to play a role for small stones of a favorable geometry. In order to test the present conjecture, numerical simulations of the flow field are employed to simulate bubble collapse near a rigid boundary. The pressure along the stone is measured over the length of the simulation and used as input into the elastic wave propagation code to evaluate the stresses within the stone.

In the present work, numerical simulations of the shock-induced collapse of a single gas bubble in water near a rigid surface are conducted. The bubble dynamics of shock-induced collapse are studied and the wall pressure, considered as a measure of potential damage via surface erosion, is characterized. In addition, the present fluid dynamics simulations are used as input into an elastic waves propagation code, in order to investigate the stresses generated within kidney stone in the context of SWL. The present work illustrates the fact that the shock-induced collapse of a gas bubble has potential not only for erosion along the stone surface, but also for structural damage within the stone.

PROBLEM SET-UP AND NUMERICAL MODEL

Since interactions between waves and interfaces constitute the main flow features of shock-induced bubble collapse, compressible multicomponent flows are considered, in which the fluid components are assumed immiscible, and diffusion, surface tension and phase change are neglected. Thus, the inviscid

and adiabatic Euler equations are solved. A stiffened equation of state is used to model water. Material interfaces are then represented by discontinuities in the fluid properties, so that advection equations for these quantities supplement the Euler system. A high-order accurate, quasi-conservative shock- and interface-capturing scheme is used to solve the governing equations. The time-marching is carried out using a third-order accurate TVD Runge-Kutta method, and the spatial discretization employs a fifth-order accurate finite volume WENO scheme in which the average primitive variables are reconstructed and for which the HLLC solver is modified to solve advection equations [11].

To simplify the problem, the expansion of the lithotripter pulse is neglected; the effect of the finite width of the pulse is investigated in Johnsen & Colonius [12]. Thus, the incoming lithotripter pulse consists of a constant-amplitude step change in pressure, p_s/p_o, with nominally zero rise time. Initially, a spherical air bubble of radius, R_o, is located at a distance, H_o, from a rigid surface. The incoming shock propagates in the direction normal to the wall, so that the problem is axisymmetric; thus, cylindrical coordinates with azimuthal symmetry are used. The range of initial stand-off distances is $1.05 \leq H_o/R_o \leq 5$ and the pressure ratio across the shock is 353, which is representative of shock wave lithotripsy. The initial bubble radius is $R_o = 50$ μm. The bubble dynamics results are non-dimensionalized using the density and sound speed of the water, and the initial bubble radius. The problem set-up is identical to that of Johnsen & Colonius [13].

The results from the computational fluid dynamics (CFD) simulations are then used as initial conditions in an elastic wave propagation code [3] in which the linear elasto-dynamics equations are solved in cylindrical coordinates using a time-domain finite difference method. There is only a one-way coupling between the fluid dynamics and the elastic waves simulations; that is, the pressure calculated from the CFD assume a rigid stone and this pressure field is then used as the input for the elastic wave code

RESULTS

Shock-bubble interaction

Upon the impact of the incoming lithotripter pulse, the bubble starts its collapse. The shock propagates around the bubble and reflects off the wall back onto the bubble, thus effectively doubling the pressure. During the collapse, a re-entrant jet forms on the surface of the bubble farthest from the wall in the direction of propagation of the shock (*i.e.*, toward the wall). At collapse, this high-speed jet impacts the distal side of the bubble and creates a strong water-hammer pressure, which then propagates outward radially and reflects off the neighboring surface. Multiple reflections between the bubble and the wall then occur. The water-hammer shock is strongest in the direction of jet impact. Clearly, shock-induced collapse is a non-spherical phenomenon, in which the detailed dynamics (*e.g.*, jet formation) are important factors in the shock emission [13]. Fig. 2 illustrates these events by showing density lines and pressure contours.

Shock-bubble interaction has been studied mainly in the context of gases [9]. In the present situation, the pressure ratio across the shock is much larger than in studies with gases – even though the shock Mach number is close to unity – so that changes in volume (*i.e.*, bubble collapse) are important factors. The interaction of the shock with the bubble is a transient process: the proximal side of the bubble is subjected to the shock sooner than the distal side, because of the finite speed of propagation of the shock. In the case of interest to SWL ($p_s/p_o = 353$), the time taken by the shock to propagate across the length of the bubble in the liquid is approximately two units; the collapse time is approximately eight units. Thus, the characteristic time relevant to the shock propagation in the liquid is not negligible compared to the characteristic time of the bubble dynamics.

To highlight certain important events in shock-induced bubble collapse, the history of the velocity of the jet, v_j, and that of the distal side, v_d, are shown in Fig. 3 for shock-induced collapse. For simplicity, collapse in a *free field* is considered for the remainder of this section. The interface is stationary until the shock reaches the proximal side, from which the jet eventually forms. Then v_j increases impulsively due to the passage of the shock ($tc_L/R_o \approx 1.4$). Until $tc_L/R_o \approx 6.0$, the velocity follows an approximately constant and small acceleration (*slow regime*); then, for $7.5 \lesssim tc_L/R_o \lesssim 9.2$, the jet velocity obeys an approximately constant and larger acceleration (*fast regime*). The large deceleration is then due to the high compression within the bubble and the impact upon the distal side. The distal side starts its motion at a later time, once the shock has diffracted around the bubble ($tc_L/R_o \approx 4.0$). Similarly to that of the proximal side, the velocity of the distal side initially obeys an approximately constant and small acceleration. However, the jet impacts it before it can ever enter the fast regime. After impact, the two sides are very close to each other, as shown in Fig. 2, and move together downstream.

In order to better understand the transient effect of shock propagation, the spherical collapse of a gas bubble (*i.e.*, free-field Rayleigh collapse) is considered. In this problem, the bubble is initially in equilibrium with its surroundings; at time 0^+, the pressure of the liquid is instantaneously raised by a pressure ratio, $p_s/p_o = 353$. It can be argued that such an idealized case can correspond to shock-induced collapse for which the shock speed is infinite; however, one main difference is the fact that the flow downstream of the shock is non-zero, whereas the flow in the liquid is initially zero in Rayleigh collapse. Fig. 4 shows the history of the velocity of the proximal and distal sides of the bubble for Rayleigh and shock-induced collapse. In order to compare the two phenomena, the initial impulsive velocity has been removed by shifting the velocity accordingly, so that the zero velocity refers to the initial conditions in all cases; in addi-

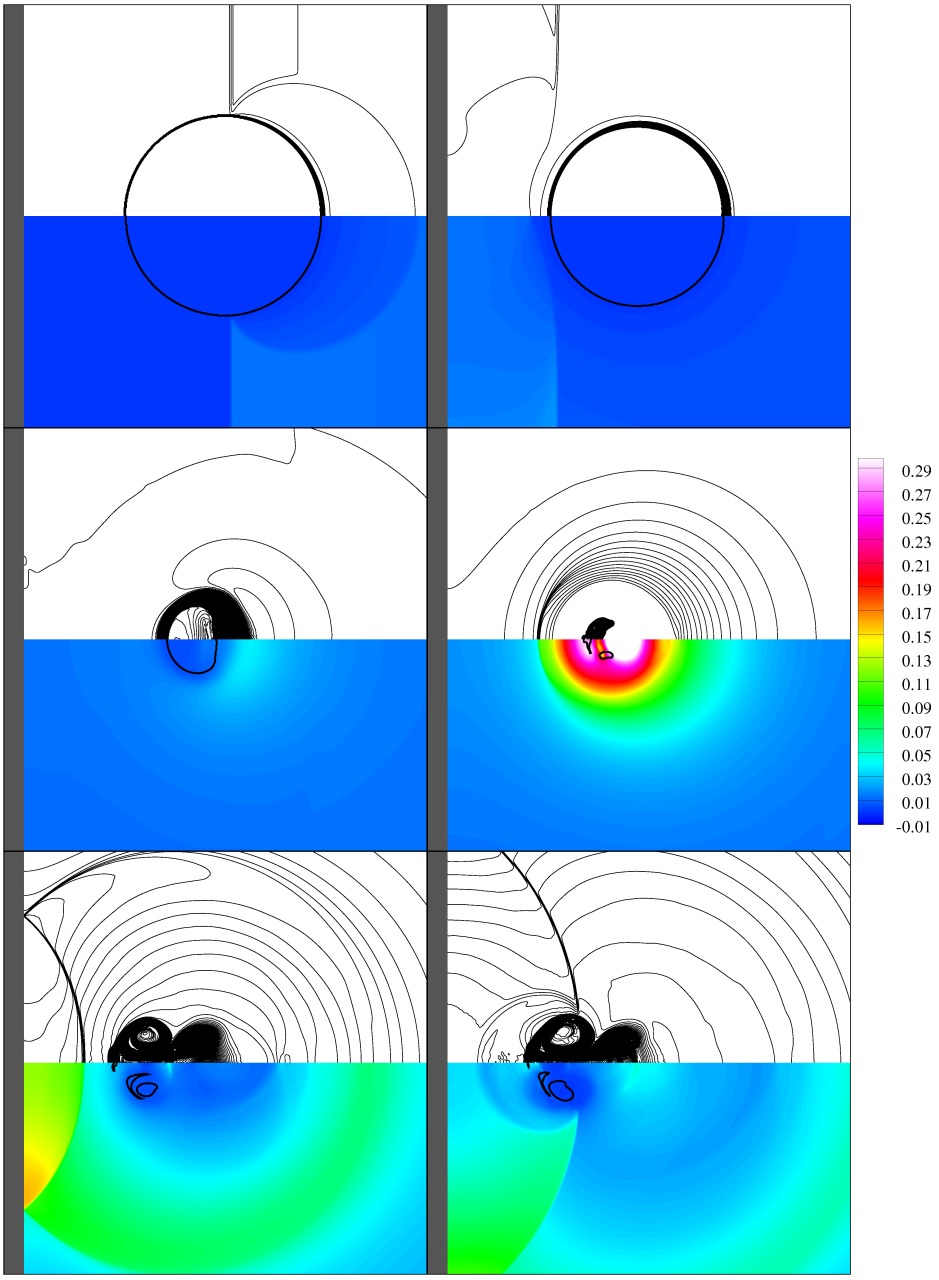

Figure 2. Density lines (top) and pressure contours with the interface outlined in black (bottom) for the shock-induced collapse of a gas bubble in shock wave lithotripsy ($p_s/p_o = 353$, $H_o/R_o = 2.0$). The pressure is non-dimensionalized by $\rho_L c_L^2$. The grey surface on the left of each frame denotes the rigid wall. Top left: the shock is diffracting around the bubble ($tc_L/R_o = 4.85$); top right: after reflecting off the wall, the shock is about to interact with the bubble again ($tc_L/R_o = 4.85$); middle left: near its collapse, the bubble is no longer spherical ($tc_L/R_o = 12.1$); middle right: after the impact of the re-entrant jet, a water-hammer shock propagates outwardg ($tc_L/R_o = 13.1$); bottomr left: the shock emitted during collapse reflects off the wall ($tc_L/R_o = 13.4$); bottom right: the reflected shock interacts with the bubble ($tc_L/R_o = 14.1$).

tion, the time origin has been shifted in shock-induced collapse, so that $t = 0$ refers to the time when the shock reaches the proximal or distal side.

The first observation is that the maximum velocity of the jet is much higher in shock-induced collapse; on the other hand, the maximum velocity of the distal side is much lower. This

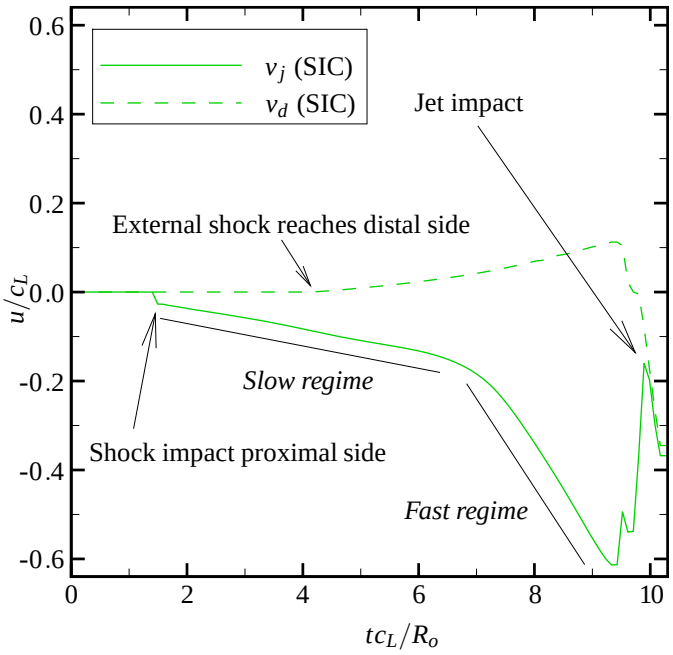

Figure 3. Velocity of the jet and of the distal side in free-field shock-induced with $p_s/p_o = 353$.

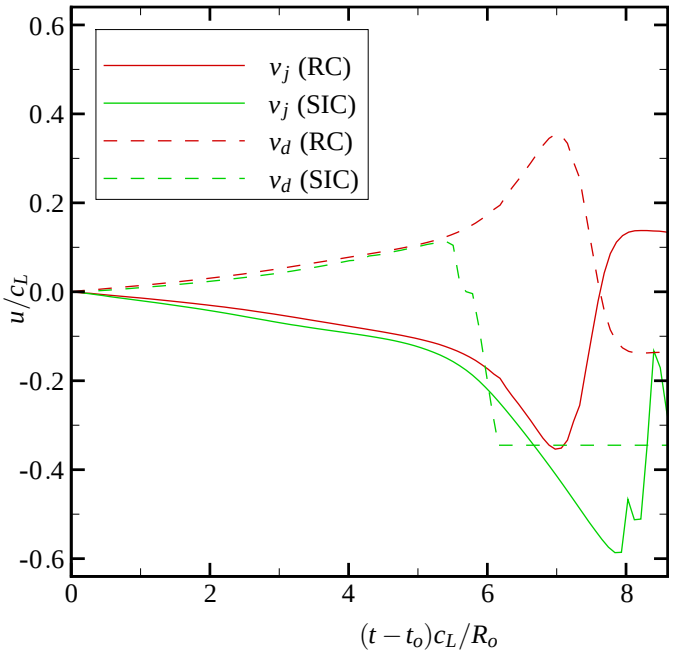

Figure 4. Comparison of the velocity of the jet and of the distal side in free-field shock-induced collapse (SIC) and Rayleigh collapse (RC) with $p_s/p_o = 353$. The time origin has been displaced for both side in the shock-induced collapse.

observation indicates the non-spherity of shock-induced collapse and emphasizes the prominence of the high-speed re-entrant jet.

Initially, the velocity of the proximal side (jet) increases more rapidly in shock-induced collapse than it does in Rayleigh collapse. After $(t-t_o)c_L/R_o \approx 3$, the acceleration is nearly the same in both cases, so that there is an approximately constant velocity difference between the two cases, until $(t-t_o)c_L/R_o \approx 5$. This velocity difference may be attributed to baroclinic vorticity, which induces a velocity on the base flow; in the case of shock-bubble interaction involving gases only [9], this phenomenon, which is an example of the Richtmyer-Meshkov instability, is clearly the mechanism responsible for the formation of the jet. After this stage, the proximal side enters the fast regime. Thus, the higher velocity allows the proximal side to enter the fast regime sooner.

By comparing the trajectories of shock-induced collapse to those of Rayleigh collapse, it is clear that the velocities of the distal side are almost identical in the two types of collapse. However, because of the delay due to the finite speed of propagation of the shock in water, the distal side is still in the slow regime when the jet impacts it. The reason for which the velocity of the proximal side (jet velocity) is higher in shock-induced collapse is clear: the proximal side accelerates in the fast regime while the distal side is still contracting slowly due to the delay; the velocity of the proximal side accelerates at the given (fast) rate and can penetrate the bubble to a greater amount because nothing is there to arrest its motion, until impact with the distal side. In the spherical case, the collapse is arrested sooner, because the trajectory of the distal side is the exact opposite of that of the proximal side. It should be noted that similar behavior is observed for different pressure ratios; these results are not shown for conciseness.

The *slow* and *fast* regimes can be better understood by considering spherical bubble collapse. Though spherical bubble dynamics are strictly not applicable to shock-induced collapse because the process is highly non-spherical, they are used to illustrate the type of effects that occur in the present simulations. For a gas bubble initially in equilibrium with its surroundings at pressure, p_o, and subjected to an instantaneous pressure rise, p_s/p_o, the Rayleigh-Plesset equation can be integrated to yield an expression for the interface velocity [1]:

$$\dot{R}^2 = \frac{2}{3}\frac{p_o}{\rho_L}\left[\frac{1}{\gamma-1}\left(\frac{R_o}{R}\right)^{3\gamma} - \frac{p_s}{p_o} + \left(\frac{p_s}{p_o} - \frac{1}{\gamma-1}\right)\left(\frac{R_o}{R}\right)^3\right], \quad (1)$$

where R is the bubble radius, R_o is the initial bubble radius, ρ_L is the density of the liquid and γ is the ratio of specific heats of the gas. Initially, whle $R(t) \approx R_o(1-\varepsilon)$, where ε is small, the

velocity obeys the following *slow* asymptotic growth:

$$\dot{R} \to -\sqrt{2\frac{p_o}{\rho_L}\left(\frac{p_s}{p_o}-1\right)\varepsilon} + O(\varepsilon^2). \tag{2}$$

On the other hand, for $R \ll R_o$, the velocity asymptotes to the following *fast* growth [1]:

$$\dot{R} \to -\left(\frac{R_o}{R}\right)^{3/2}\sqrt{\frac{2}{3}\frac{p_o}{\rho_L}\left[\frac{p_s}{p_o}-\frac{1}{\gamma-1}\left(\frac{R_o}{R}\right)^{3(\gamma-1)}\right]}. \tag{3}$$

The maximum velocity of the jet and of the distal side are important quantities, because the impact of the jet onto the distal generates a water-hammer shock. This shock then propagates outward and impacts any neighboring surface, as explained in the next section; the amplitude of this shock is directly proportional to the velocity difference between the jet and the distal side.

Pressure measurements along a rigid surface

In the present section, the potential of shock-induced bubble collapse for surface erosion is illustrated based on the results of Johnsen & Colonius [13].[1] The pressure history measured along the neighboring rigid surface is shown in Fig. 5 for two different radial distances from the centerline. First, the incoming shock impacts the wall at $tc_L/R_o \approx 7$. Because of the presence of the bubble, the shock lags slightly along the centerline. After reflection off the wall, the shock interacts with the bubble again. Because of the impedance mismatch, the reflected wave is an expansion wave, so that a dip is observed in the profile at $tc_L/R_o \approx 9$. Thereafter, the pressure increases significantly due to the shock emitted upon bubble collapse. The pressure amplitude decreases at a larger distance away from the centerline, because the shock is propagating radially outward. After reflection off the wall, this shock interacts with the bubble and inverts its amplitude due to the impedance mismatch. Thus, regions of tension (*i.e.*, negative pressure) are observed. Multiple reflections then occur between the bubble and the wall.

In order to quantify the potential damage of this process, the maximum wall pressure, $p_{wall,max}$, generated over the course of the simulation is measured and plotted as a function of the location of the bubble upon collapse, H_c, in Fig. 6. H_c is determined by calculating the distance between the bubble centroid and the wall. Very high pressures are achieved (up to 2.3 GPa) for bubbles initially close to the wall. As expected [10], the pressure along the centerline decreases as $1/r$. In other words, the shock strength decreases with distance from the origin of the shock. At

[1]Figs. 5-6 are adapted from [13]. Copyright 2003 by Cambridge University Press.

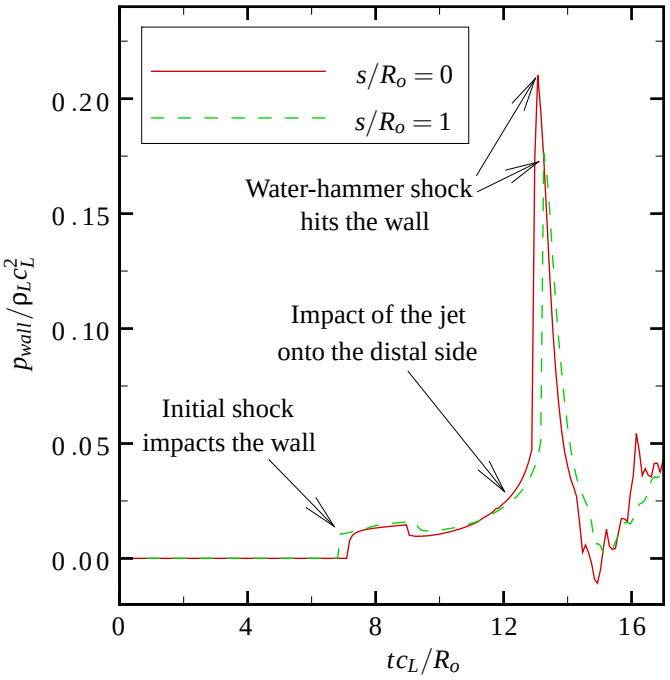

Figure 5. History of the wall pressure at different locations along the wall for shock-induced collapse near a wall ($p_s/p_o = 353$, $H_o/R_o = 2.0$).

a farther radial distance along the wall ($s/R_o = 1$), the behavior of the pressure is different, in that the pressure is smaller for bubbles closer to the wall. This discrepancy can be explained by the fact that the shock emitted upon collapse propagates radially outward and reflects off the wall at an acute angle, thus leading to a lower pressure than expected in normal shock reflection. An important observation is that, for bubbles initially close enough to the wall, the shock emitted upon collapse is stronger than the incoming lithotripter pulse; in non-dimensional units, the pulse amplitude is 1.29×10^{-2}. In fact, by extrapolating from the $1/r$ curve in Fig. 6, the shock emitted upon collapse is as strong as the incoming shock provided the bubble is initally within a distance of eight initial radii from the wall.

For a given initial stand-off distance, the extent over which the pressure due to bubble collapse is larger than that of the lithotripter shock can be estimated assuming the shock is normal (*i.e.*, for bubbles not too close to the wall) and using basic geometry. The pressure along the wall surface is given by [12]:

$$p_{wall} = \frac{c_1}{\sqrt{H_c^2 + s^2}} + c_2, \tag{4}$$

where s is the radial distance along the wall, H_c is the location of the bubble upon collapse for a given initial stand-off distance, H_o, and c_1 and c_2 are constant that can be determined if at least two measurements are known. For the case, $H_o/R_o = 2.0$, the

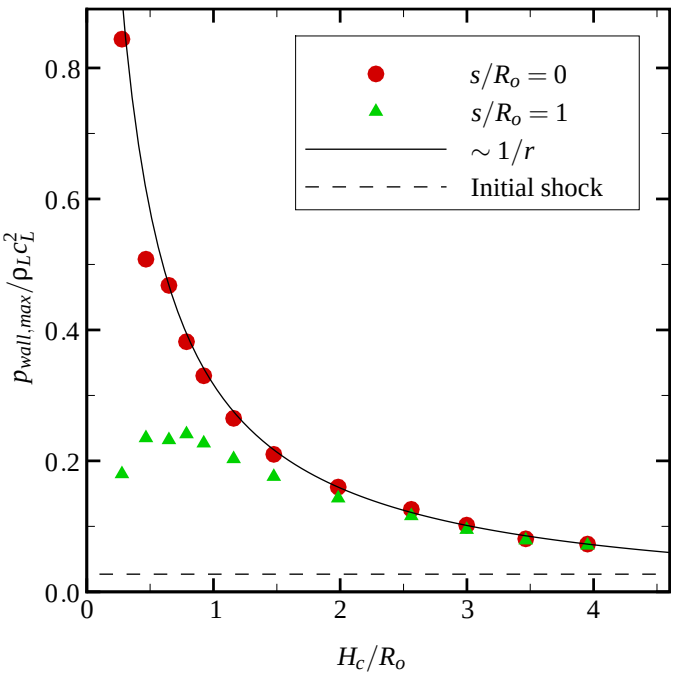

Figure 6. Maximum wall pressure at different distances from the centerline ($s = 0$) as a function of the location of the collapse, H_c, for shock-induced collapse ($p_s/p_o = 353$). H_c is determined by calculating the distance between the centroid of the bubble to the wall.

distance along the wall for which the pressure is as large as that due to the incoming shock is $10R_o$. The agreement between this model and the simulation results is very good [12, 13].

Wave propagation in kidney stones

In the previous section, the potential of shock-induced bubble collapse for the erosion of neighboring surface was characterized. The pressures measured in this process exceed those estimated by Philipp & Lauterborn [14], in which surface erosion was studied and observed for Rayleigh collapse of vapor bubbles, and therefore are significant enough to lead to surface erosion regardless of the stone size and shape. Since the pressures are so large, they may have the potential to cause failure by mechanisms similar to the direct action of the lithotripter pulses on the stone, *e.g.*, interference of shear and surface waves [3], squeezing [7], or spallation [19].

The pressure generated by bubble collapse along a neighboring stone may be much larger locally than that due to the incoming lithotripter pulse; however, the amplitude of the shock decays as $1/r$. Since the shock emitted upon collapse propagates through the stone, effects similar to those that occur during the interaction of the lithotripter pulse with the stone are expected to be observed. However, because the pressure decays as $1/r$, the effects described previously may not be substantial for all stones; particularly, such effects would be more significant for smaller stones of a favorable shape. This phenomenon may explain why the combined effect of shock propagation within the stone and cavitation leads to the most efficient stone comminution rate.

To verify this hypothesis, the computational fluid dynamics (CFD) simulations are prescribed as an initial condition for the propagation of elastic waves within the stone, using the code of Cleveland & Sapozhnikov [3]. In this model, the kidney stone is assumed to behave as a linear, isotropic, elastic solid, so that the resulting elasto-dynamics equations solved using a time-domain finite difference method (FDTD). In the elastic waves simulations, the computational domain consists of a kidney stone immersed in water. For the water, the density is 1000 kg/m^3 and the sound speed in water is 1500 m/s, and for the stone, the density is 1700 kg/m^3, the compressional wave speed is 2635 m/s and the shear wave speed is 1328 m/s. The pressure along the stone surface is given from the hydrodynamic simulations as a time-varying boundary condition; however, it is transformed into an initial condition in the water for the elastic waves simulations of the form, $f(t - x/c_L)$, where c_L is the sound speed in water. The boundary conditions at $x = 0$ (*i.e.*, the stone surface) corresponds to $f(t)$, so that the initial spatial distribution becomes $f(-x/c_L)$. The wave propagation within the stone does not affect the wall pressure; in other words, there is only a one-way coupling between the hydrodynamics and the wave propagation in the stone.

In order to illustrate the propagation of the shock emitted during shock-induced collapse within the stone, pressure contours are plotted in Figure 7 for a cylindrical stone (radius: $R_{stone} = 3.5$ mm; length: $L_{stone} = 7.5$ mm). The bubble is aligned with the longitudinal axis of the cylinder and is initially located at a distance $H_o/R_o = 1.5$ below the stone, where $R_o = 100$ μm. The outline of the stone is included.

The initial conditions are shown in frame 1 (0 μs). The shock generated by bubble collapse is partly transmitted as a shock into the stone and partly reflected as a shock back into the water; because of the higher sound speed in the stone, the wave propagates faster therein (1 μs). The initial shock propagates radially outward, so that it reflects off the sides of the stone and then intersects along the centerline (2 μs). In the meantime, the shock in water diffracts around the edge of the stone and leads to the formation of shear waves. The main front reflects off the distal side (3 μs) and inverts its amplitude since the end of the stone acts as a pressure-release surface, thus the reflected wave leads with a tensile phase (4 μs). Furthermore, the different types of waves (*e.g.*, reflected, shear, surface) interact with each other within the stone to produce other localized regions of tension (5 μs). It should be noted that the amplitude of the stresses becomes smaller in each frame, as expected since the initial shock generated by the bubble collapse decreases as $1/r$. Hence, higher tensile stresses are expected to be generated in small stones. In addition, a geometry that favors shock focusing within the stone (*e.g.*, a sphere) is

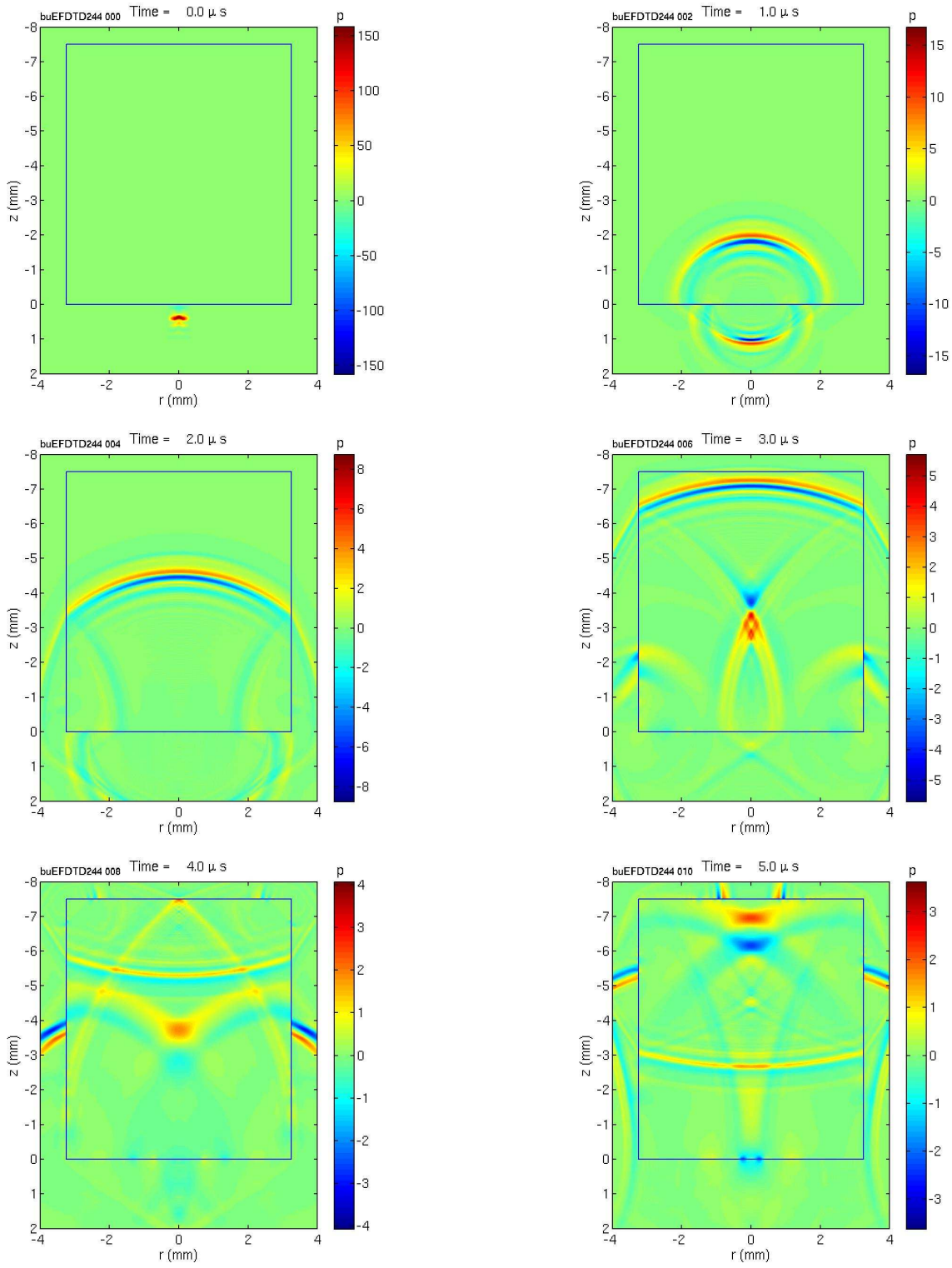

Figure 7. Snapshots of the pressure distribution for the case of a cylindrical stone (radius: 3.5 mm; length: 7.5 mm). The pressure within the stone is calculated as the trace of the stress tensor. The time intervale between each frame is 1 μs. The color scale is in MPa and is adjusted on each frame to the peak pressure.

expected to generate higher stresses.

In order to understand the effect of stone size and geometry on the tensile stress inside the stone, the principal stresses were calculated throughout the simulation and the peak tensile stress recorded at each location in the stone. Figure 8 shows the distribution of the peak tensile stress for a small ($R_{stone} = 1$ mm) and larger ($R_{stone} = 2$ mm) spherical stone. The units for the stresses are MPa, and the white line denotes the stone outline. Again, the bubble is initially located at $H_o/R_o = 1.5$ below the stone, with $R_o = 100$ μm.

On the proximal surface, both cases show similar regions of high tension. This is expected, because the initial conditions based on the bubble collapse are identical; the only difference is the curvature of the stone. The reason for the high tension (as opposed to the previously discussed high compression) is as follows. The shock generated upon bubble collapse reflects off the stone back onto the bubble. As it subsequently reflects off the bubble, the amplitude of the shock inverts, thereby generating the large tension in the water on the proximal side of the stone.

The stress contours within the stone are different in the two cases, because of the different geometry. The shock generated upon collapse propagates through the stone. Because of the shock reflection off the distal side and of the interference of the shear and surface waves, a high tension (approximately 100 MPa) is observed near the distal side of the stone. As expected, this effect is enhanced in the smaller stone; because the amplitude of the shock strength decays as $1/r$ within the stone as well, the amplitude of the shock at the end of the stone is higher if the stone is smaller. The spherical geometry achieves larger stresses because of the focusing of the waves. Kidney stones typically have tensile strengths (under static testing) on the order of 1 MPa [4], so that this effect is expected to be important.

CONCLUSIONS

In the present work, numerical simulations are used to study the shock-induced collapse of a gas bubble near a rigid surface. The bubble dynamics of shock-induced collapse are first studied; it is shown that the transient nature of the shock propagation in water is important for the bubble dynamics. The pressure generated by shock-induced bubble collapse is characterized; this phenomenon leads to high compressive stresses on the proximal surface of kidney stones, thus exhibiting strong potential for surface erosion [14, 17]. In addition, the propagation of the shock generated upon collapse may lead to damage within the stone. Based on the present results, a more comprehensive understanding of stone comminution in SWL is presented: (i) Spallation, squeezing, and/or shear and surface waves due to the incoming lithotripter pulse break the stone into smaller bits, (ii) High tensile regions within the stone due to the shock generated by bubble collapse further fragments the remaining small pieces, and (iii) Cavitation erosion grinds the resulting pieces to an even smaller size. Thus, shock-induced bubble collapse has significant potential for erosion along the stone surface, and may lead to structural damage within the stone as well.

By using CFD results of shock-induced bubble collapse and elastic wave propagation simulations within the stone, the present work shows that surface erosion and internal damage to neighboring structures may be generated by the shock emitted upon bubble collapse. This provides an explanation as to how the combined effect of bubble collapse and wave propagation may work in synergy to provide the most efficient comminution of kidney stones. Further studies involve considering a finite sized stone in the CFD calculations and study the effect stone shape. In order to obtain a more complete picture of the damage caused by bubbles to structures in general and kidney stones in particular, Rayleigh collapse of vapor bubbles should be studied; numerical methods that include phase change are presently being developed.

ACKNOWLEDGEMENTS

The authors gratefully acknowledge helpful discussions with members of the Consortium for Shock Waves in Medicine. The present work was supported by by NIH Grant PO1 DK043881 (Andrew Evan PI) and ONR Grant N00014-06-1-0730.

REFERENCES

[1] C. E. Brennen, *Cavitation and bubble dynamics*, Oxford University Press, Oxford, UK, 1995.

[2] C. Chaussy, *Extracorporeal shock wave lithotripsy*, Karger, Basel, Switzerland, 1982.

[3] R. Cleveland and O. A. Sapozhnikov, *Modeling elastic wave propagation in kidney stones with application to shock wave lithotripsy*, J. Acoust. Soc. Am. **118** (2005), 2667–2676.

[4] N. P. Cohen and H. N. Whitfield, *Mechanical testing of urinary calculi*, Wolrd J. Urol. **11** (1993), 1–18.

[5] A. J. Coleman, J. E. Saunders, L. A. Crum, and M. Dyson, *A survey of the acoustic output of commercial extracorporeal shock wave lithotripsy*, Ultrasound Med. Bio. **13** (1987), 69–76.

[6] L. A. Crum, *Cavitation microjets as a contributory mechanism for renal calculi disintegration in ESWL*, J. Urol. **140** (1988), 1587–1590.

[7] W. Eisenmenger, *The mechanisms of stone fragmentation in eswl*, Ultrasound Med. Bio. **27** (2001), 683–693.

[8] S. M. Gracewski, G. Dahake, Z. Ding, S. J. Burns, and E. C. Everbach, *Interal stress wave measurements in solids subjected to lithotripter pulses*, J. Acoust. Soc. Am. **94** (1993), 652–661.

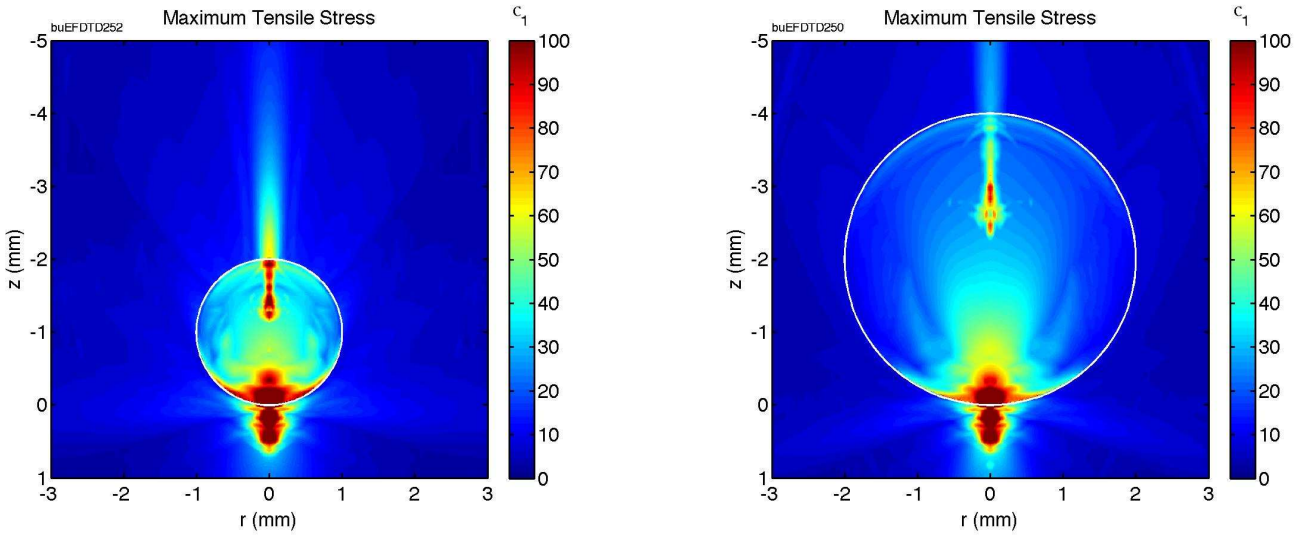

Figure 8. Maximum tensile stress calculated in spherical stones (Left: $R_{stone} = 1$ mm; right: $R_{stone} = 2$ mm). For the small stone, a region of higher tensile stress occurs near the distal surface.

[9] J. F. Haas and B. Sturtevant, *Interaction of weak shock waves with cylindrical and spherical gas inhomogeneities*, J. Fluid Mech. **181** (1987), 41–76.

[10] R. Hickling and M. S. Plesset, *Collapse and rebound of a spherical bubble in water*, **7** (1964), 7–14.

[11] E. Johnsen and T. Colonius, *Implementation of WENO schemes for compressible multicomponent flow problems*, J. Comput. Phys. **219** (2006), 715–732.

[12] _____, *Shock-induced collapse of a gas bubble in shock-wave lithotripsy*, J. Acoust. Soc. Am. **124** (2008), 2011–2020.

[13] _____, *Numerical simulations of non-spherical bubble collapse*, J. Fluid Mech. **629** (2009), 231–262.

[14] A. Philipp and W. Lauterborn, *Cavitation erosion by single laser-produced bubbles*, J. Fluid Mech. **361** (1998), 75–116.

[15] Y. A. Pishchalnikov, O. A. Sapozhnikov, M. R. Bailey, J. C. Williams, R. O. Cleveland, T. Colonius, L. A. Crum, A. P. Evan, and J. A. McAteer, *Cavitation bubble cluster activity in the breakage of kidney stones by lithotripter shockwaves*, J. Endourol. **17** (2003), 435–446.

[16] M. S. Plesset and R. B. Chapman, *Collapse of an initially spherical vapour cavity in the neighbourhood of a solid boundary*, J. Fluid Mech. **47** (1971), 283–290.

[17] Y. Tomita and A. Shima, *Mechanisms of impulsive pressure generation and damage pit formation by bubble collapse*, J. Fluid Mech. **169** (1986), 535–564.

[18] C. K. Turangan, A. R. Jamaluddin, G. J. Ball, and T. G. Leighton, *Free-Lagrange simulations of the expansion and jetting collapse of air bubbles in water*, J. Fluid Mech. **598** (2008), 1–25.

[19] X. Xi and P. Zhong, *Dynamic photoelastic study of the transient stress field in solids during shock wave lithotripsy*, J. Acoust. Soc. Am. **109** (2001), 1226–1239.

[20] S. Zhu, F. H. Cocks, G. M. Preminger, and P. Zhong, *The role of stress waves and cavitation in stone comminution in shock wave lithotripsy*, Ultrasound Med. Bio. **28** (2002), 661–671.